Crystal Morphology

Opposite Face Sensitivity of CeO_2 in Hydrogenation and Oxidation Catalysis

Gianvito Vilé, Sara Colussi, Frank Krumeich, Alessandro Trovarelli,* and Javier Pérez-Ramírez*

Abstract: *The determination of structure–performance relationships of ceria in heterogeneous reactions is enabled by the control of the crystal shape and morphology. Whereas the (100) surface, predominantly exposed in nanocubes, is optimal for CO oxidation, the (111) surface, prevalent in conventional polyhedral CeO_2 particles, dominates in C_2H_2 hydrogenation. This result is attributed to the different oxygen vacancy chemistry on these facets. In contrast to oxidations, hydrogenations on CeO_2 are favored over low-vacancy surfaces owing to the key role of oxygen on the stabilization of reactive intermediates. The catalytic behavior after ageing at high temperature confirms the inverse face sensitivity of the two reaction families.*

Although the majority of industrial catalysts are based on nanoparticles of poorly defined morphology, theoretical and experimental studies have recognized that the activity and selectivity of a structure-sensitive reaction can be enhanced by engineering the shape and tailoring the size of the nanocrystals.[1] Ceria (CeO_2), for example, plays an important role as a catalyst[2] or promoter[3] in a variety of reactions, including the steam reforming of oxygenates and the oxidation of different compounds, such as CO, HCl, and soot. The success of CeO_2 in these applications is tightly linked to its oxygen storage capacity (OSC) and the flexible transition between the Ce^{3+} and Ce^{4+} oxidation states, forming and annihilating oxygen vacancies in a stable fluorite-type structure.[2a,4] These properties, which in turn are associated with the arrangement of the terminated surface oxygen atoms, greatly depend on the morphology of the ceria crystals.[5] In fact, compared to ceria nanoparticles, which are dominated by (111) surfaces, single-crystalline nanocubes expose (100) facets, showing a lower formation energy of oxygen vacancies[6] and a different nature and amount of defect sites. This results in higher oxygen mobility and storage, and thus enhanced oxidation activity.[2b,c,e]

The emergence of CeO_2 as an ultra-selective catalyst for gas and liquid-phase semi-hydrogenation of acetylenic compounds has opened a new field of research for this intriguing rare earth oxide.[7] This is due to the practical relevance of this reaction for the purification of olefin streams and for the manufacture of fine chemicals and pharmaceuticals. Experimental observations have pointed to the adverse effect of the oxygen vacancies created by pre-reduction of CeO_2 in H_2 flow on the alkyne hydrogenation activity.[7a] Density functional theory (DFT) simulations have supported this result, showing that the presence of surface oxygen atoms is crucial for stabilizing reactive species, such as acetylene and hydrogen.[8] Notwithstanding, no study has analyzed the relationship between the oxygen storage capacity, the crystal morphology, and the hydrogenation performance. In this work, we present activity correlations with the crystal shape and exposed surface planes of nanoscale ceria in acetylene hydrogenation and CO oxidation. This enables a better understanding of the structure–performance relationships of cerium oxide in hydrogenation reactions, and establishes the bridge between hydrogenation and oxidation catalysis on CeO_2.

Ceria samples of variable morphology were prepared by precipitation (conventional nanoparticles, code CV) and hydrothermal synthesis for 24 h (nanocubes, code NC).[2e] Furthermore, the hydrothermal route was interrupted after 15 h to obtain a material containing a mixed morphology of both nanoparticles and nanocubes (code MX). Prior to catalytic use, the samples were calcined at different temperature (723–823 K) to attain materials with similar textural properties (Table 1). These samples are denoted as fresh catalysts (code -f). X-ray diffraction (XRD) confirms that CeO_2 is the only crystalline phase (Supporting Information, Figure S1), and the broadening of the diffraction peaks of CV-f compared to MX-f and NC-f indicates a decrease of the average crystallite size (Table 1). The absence of impurities of other metals in the samples was verified by inductively coupled plasma mass spectrometry (ICP-MS). High-resolution transmission electron microscopy (HRTEM; Figure 1) reveals that the fresh CV-f sample is characterized by irregularly shaped polyhedral CeO_2 particles of variable diameter (10–40 nm). The dominant lattice fringes (0.32 nm) correspond to the (111) family, and only a few (100) facets were detected. This is compatible with the shape of most particles defined by an octahedron-like geometry and a minority described by a truncated octahedron enclosed by (111) and (100) facets, in accordance with other studies.[9] NC-f, on the other hand, displays nanocubes of different size (15–60 nm). The presence of crystallographic planes of CeO_2 with characteristic 0.27 nm interplanar spacing reveals that the

[*] G. Vilé, Dr. F. Krumeich, Prof. J. Pérez-Ramírez
Institute for Chemical and Bioengineering
Department of Chemistry and Applied Biosciences, ETH Zurich
Vladimir-Prelog-Weg 1, 8093 Zurich (Switzerland)
E-mail: jpr@chem.ethz.ch

Dr. S. Colussi, Prof. A. Trovarelli
Department of Chemistry, Physics, and Environment
University of Udine
Via del Cotonificio 108, 33100 Udine (Italy)
E-mail: trovarelli@uniud.it

Supporting information for this article is available on the WWW under http://dx.doi.org/10.1002/anie.201406637.

Table 1: Characterization and catalytic performance of the ceria samples.

Sample	Method	Activation	S_{BET} [$m^2 g^{-1}$]	V_{pore} [$cm^3 g^{-1}$]	$d_{crystallite}$ [nm]	H_2 consumption[a] [$cm^3 H_2 g\,CeO_2^{-1}$]	OSC[b] [$\mu mol\,O\;m^{-2}$]	$r_{hydrogenation}$[c] [$\mu mol\,C_2H_4\;h^{-1}\,m^{-2}$]	$r_{oxidation}$[c] [$\mu mol\,CO_2\;h^{-1}\,m^{-2}$]
CV-f	precipitation	air, 823 K, 2 h	34	0.30	18	1.73	0.4	14	38
CV-a	precipitation	air, 1023 K, 4 h	3	0.11	60	0.36	0.9	8	141
MX-f	hydrothermal, 15 h	air, 723 K, 2 h	29	0.28	24	2.37	n.a.	12	78
MX-a	hydrothermal, 15 h	air, 1023 K, 4 h	8	0.14	38	1.85	n.a.	6	217
NC-f	hydrothermal, 24 h	air, 723 K, 2 h	29	0.31	28	2.49	6.8	9	142
NC-a	hydrothermal, 24 h	air, 1023 K, 4 h	11	0.16	34	2.08	11.2	4	329

[a] Calculated from the H_2-TPR profile up to 673 K. [b] Calculated from TGA in H_2 flow at 673 K.[2e] [c] $T = 473$ K.
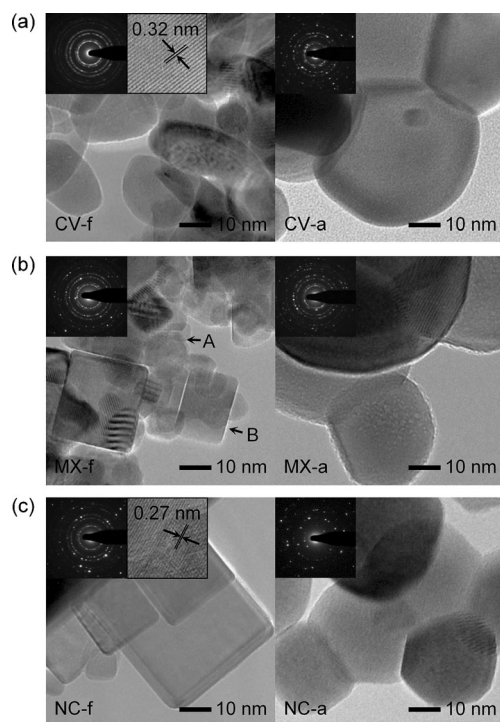

Figure 1. High-resolution transmission electron microscopy, revealing staggering morphological differences between the fresh samples (left), from octahedral and truncated nanoparticles (a) to nanocubes (c). The samples after aging at 1023 K (right) show the alteration of the catalyst morphology and the aggregation of the ceria particles. Insets: selected-area diffraction pattern of each catalyst and, in the case of CV-f and NC-f, the interplanar spacing of the crystallographic planes of CeO_2.

particles are single-crystalline and enclosed by six (100) facets. Finally, the MX-f catalyst contains both conventional (A) and cubic (B) ceria particles. The morphology differences among the catalysts bring variable redox properties. In fact, temperature-programmed reduction with H_2 (H_2-TPR) of CV-f shows two major peaks at about 750 and above 1000 K (Figure 2), attributed to the reduction of the surface and bulk of the ceria crystal, respectively.[2a] As the amount of cubic particles in the sample increases, the surface peak shifts towards lower temperatures, indicating that the nanocubes are more easily reduced. The enhancement of the redox

behavior observed by H_2-TPR is in line with the higher oxygen storage capacity of the nanocubes compared to the conventional powder (Table 1).[2b,e]

The fresh CeO_2 samples were subjected to a high-temperature calcination (1023 K) leading to the so-called aged catalysts (code -a). As shown in Table 1, the surface area and pore volume drop to values lower than $11\;m^2 g^{-1}$ and $0.16\;cm^3 g^{-1}$, respectively. HRTEM reveals that the thermal treatment alters the crystal morphology, leading to conventional nanoparticles and aggregated, truncated cubes (Figure 1). This results in an increase of (100) facets on conventional ceria and in the formation of (110) and higher Miller index surfaces on ceria nanocubes. In the H_2-TPR profile (Figure 2), a slight shift towards lower temperatures and a decrease in the intensity of the surface reduction peak are observed in all aged samples; this is accompanied by an increase in the intensity of the peak associated with the bulk reduction of the sample, in agreement with the decreased surface area. The storage behavior also improves with ageing, indicating that the catalysts activated at high temperature readily exchange oxygen with the environment.[2e]

Figure 3 compares the acetylene hydrogenation performance of standard, mixed, and cubic CeO_2 in the temperature range of 323–623 K. The reaction rate resembles a volcano behavior over all catalysts, increasing when the temperature is increased from 323 to about 523 K and dropping at higher temperatures. Earlier reports have attributed this decrease to the unfavorable reduction of the ceria surface.[7] In general, the hydrogenation activity follows the order: CV-f > MX-f > NC-f. The selectivity to ethylene, on the other hand, is constant at 80% in all cases, although at low temperatures
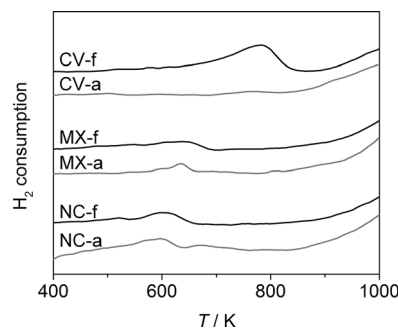

Figure 2. Characterization of the fresh and aged ceria samples by temperature-programmed reduction with hydrogen.
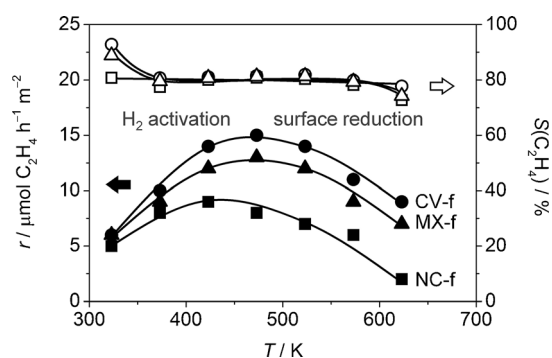
Figure 3. Reaction rate (solid symbols) and selectivity to ethylene (open symbols) of the ceria catalysts in C_2H_2 hydrogenation at variable temperature.

CV-f outperforms MX-f and NC-f. This is most likely because of the better isolation of the terminated surface oxygen atoms on CeO_2(111) (see the inset in Figure 4), which reduces the likelihood of oligomer formation.[8] Notably, the catalyst morphology is preserved after C_2H_2 hydrogenation (Supporting Information, Figure S2), confirming that these results are not a consequence of nanoparticle shape changes induced by the reaction. The similar alkene selectivity over all catalysts is consistent with the analogous apparent activation energy (14 kJ mol^{-1} for NC-f and 15 kJ mol^{-1} for MX-f and CV-f), indicating that this structure sensitivity cannot be attributed to different elementary steps in the reaction mechanism. Comparatively, the same materials exhibit an opposite activity trend in CO oxidation (Table 1; Supporting Information, Figure S3), with the nanocubes being the most active. The C_2H_2 hydrogenation and CO oxidation activity are further compared as a function of the oxygen storage capacity in Figure 4. The figure depicts the antithetic shape sensitivity of these reactions over nanoscale ceria. In fact, the hydrogenation rate decreases with the increased OSC and the effect is even more pronounced over the aged samples; CO oxidation is favored at high oxygen storage capacities and over the aged materials.
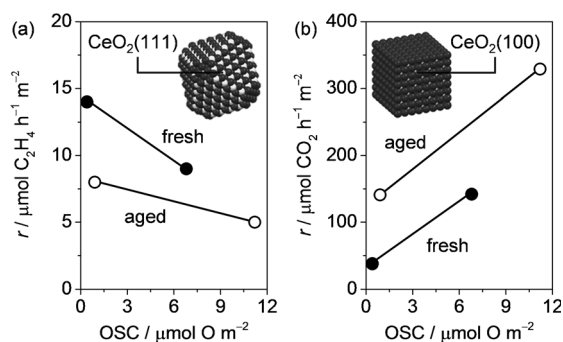

Figure 4. Reaction rate in C_2H_2 hydrogenation (a) and CO oxidation (b) as a function of the oxygen storage capacity (OSC) of the fresh and aged ceria catalysts. Both reactions were investigated at $T = 473$ K. Insets: the most active CeO_2 morphology in C_2H_2 hydrogenation (octahedron-like nanoparticles enclosed by (111) facets) and CO oxidation (nanocubes enclosed by (100) facets). O dark gray, Ce light gray.

The inverse structure sensitivity of CeO_2 in hydrogenation and oxidation can be attributed to the different oxygen vacancy chemistry and to the nature of the exposed facets. In general, the formation energy of oxygen vacancies on CeO_2-(111) is higher (3.30 eV) than on CeO_2(100) (2.97 eV),[6] suggesting that the oxygen atoms on CeO_2(111) are less volatile. Therefore, the hydrogenation performance, which is higher on the (111) facets of the conventional nanoparticles, can be associated with a mechanism requiring surface oxygen atoms to stabilize reactive species, which is consistent with the recently proposed acetylene hydrogenation mechanism over ceria.[8a] To the best of our knowledge, this also shows for the first time the detrimental role of the (100) planes in reactions catalyzed by ceria. On the other hand, CO oxidation depicts the opposite trend, with the (100) surfaces being more active, in agreement with previous reports and with a mechanism involving surface oxygen removal.[2c, 10] The ageing experiment confirms these results, as the hydrogenation rate in conventional octahedral nanoparticles decreases for all samples, because of the formation of new (100) planes from truncation of the CeO_2 particles. In contrast, a parallel increase of the CO oxidation activity is observed. In nanocubes, ageing results in a modification of the edges and corners with exposure of new (110) planes and other planes with higher Miller indices. This will also favor the energetics of vacancy creation (the vacancy formation energy in (110) plane is 2.69 eV[6b]) and the formation of defects and coordinatively unsaturated sites (where oxygen is more reactive), promoting specific rate of CO oxidation over aged samples. Conversely, hydrogenation rates are negatively affected by ageing.

In conclusion, we have compared the shape-dependent activity of ceria nanocatalysts with cubic and conventional morphologies in C_2H_2 hydrogenation and CO oxidation. The material exposing (111) facets shows a higher hydrogenation activity while the (100) surfaces dominate in the oxidation reaction. The ageing at high temperature induces a strong alteration of the catalyst morphology, increasing the amount of (100) facets in conventional samples and (110) facets in nanocubes, improving the oxygen storage capacity of the samples. Consequently, these catalysts appear to be more active in oxidation rather than in hydrogenation. This can be related to the easier formation of ceria oxygen vacancies and defect sites on CeO_2(100), which are adverse in C_2H_2 hydrogenation and active species in CO oxidation, and suggests opposite criteria for the design of ceria catalysts for hydrogenation and oxidation reactions. These results provide a method to assess the structure sensitivity of heterogeneous catalysts, which is a critical step in catalyst design, and enable a better understanding of the relationship between the oxygen storage capacity, the crystal morphology, and the catalytic performance of CeO_2 in these reactions.

Experimental Section

Conventional CeO_2 nanoparticles were prepared by precipitation of a $Ce(NO_3)_3 \cdot 6H_2O$ (Treibacher Industrie AG) solution with NaOH, followed by filtration and washing. The nanocubes were prepared by precipitation of a cerium nitrate solution with NaOH, followed by

hydrothermal treatment in a Teflon-lined stainless-steel autoclave at 453 K for 24 h. After cooling, the mixture was centrifuged and then washed in a water/ethanol mixture for purification. Mixed samples were obtained by quenching the hydrothermal treatment after 15 h, followed by filtration and extensive washing. Afterwards, all of the materials were dried overnight at 333 K, and calcined in static air at 723–823 K for 2 h (fresh samples) and at 1023 K for 4 h (aged samples). Details on the characterization methods are given in the Supporting Information. The gas-phase hydrogenation of acetylene was studied in a continuous-flow fixed-bed micro-reactor (12 mm i.d.)[7a, 8a] using the following conditions: catalyst mass $W_{cat} = 0.25$ g (particle size $= 0.2$–0.4 mm), temperature $T = 423$–673 K, contact time $\tau = 1$ s, $H_2/C_2H_2 = 30$ (acetylene concentration $= 2.5$ vol %, He as balance gas), and total pressure $P = 1$ bar. The reactor effluent was analyzed by an online gas chromatograph (Agilent GC7890A). CO oxidation was carried out in a continuous-flow fixed-bed microreactor (6 mm i.d.), using: $W_{cat} \approx 0.03$ g (powder), $T = 298$–593 K (heating rate $= 10$ K min^{-1}), $O_2/CO = 2.5$ (CO concentration $= 2$ vol %, He as balance gas), $F = 50$ cm^3 min^{-1}, and $P = 1$ bar. The effluent gases were continuously analyzed by an ABB Uras 14 infrared gas analyzer. The conversion of C_2H_2 (CO) was determined as the amount of reacted C_2H_2 (CO) divided by the amount of C_2H_2 (CO) at the reactor inlet. The reaction rate was expressed as micromoles of C_2H_2 (CO) per unit of time and surface area. The selectivity to ethylene was calculated as the amount of ethylene formed divided by the amount of converted acetylene.

[1] a) C. J. Murphy, *Science* **2002**, *298*, 2139; b) Y. Xia, Y. Xiong, B. Lim, S. E. Skrabalak, *Angew. Chem.* **2009**, *121*, 62; *Angew. Chem. Int. Ed.* **2009**, *48*, 60; c) K. Zhou, Y. Li, *Angew. Chem.* **2012**, *124*, 622; *Angew. Chem. Int. Ed.* **2012**, *51*, 602.

[2] a) A. Trovarelli, *Catal. Rev. Sci. Eng.* **1996**, *38*, 439; b) D. Y. Wang, Y. J. Kang, V. Doan-Nguyen, J. Chen, R. Kungas, N. L. Wieder, K. Bakhmutsky, R. J. Gorte, C. B. Murray, *Angew. Chem.* **2011**, *123*, 4470; *Angew. Chem. Int. Ed.* **2011**, *50*, 4378; c) K. Zhou, X. Wang, X. Sun, Q. Peng, Y. Li, *J. Catal.* **2005**, *229*, 206; d) A. P. Amrute, C. Mondelli, M. Moser, G. Novell-Leruth, N. López, D. Rosenthal, R. Farra, M. E. Schuster, D. Teschner, T. Schmidt, J. Pérez-Ramírez, *J. Catal.* **2012**, *286*, 287; e) E. Aneggi, D. Wiater, C. de Leitenburg, J. Llorca, A. Trovarelli, *ACS Catal.* **2014**, *4*, 172.

[3] a) S. Park, J. M. Vohs, R. J. Gorte, *Nature* **2000**, *404*, 265; b) G. A. Deluga, J. R. Salge, L. D. Schmidt, X. E. Verykios, *Science* **2004**, *303*, 993; c) B. M. Reddy, P. Bharali, P. Saikia, A. Khan, S. Loridant, M. Muhler, W. Grünert, *J. Phys. Chem. C* **2007**, *111*, 1874.

[4] a) F. Esch, S. Fabris, L. Zhou, T. Montini, C. Africh, P. Fornasiero, G. Comelli, R. Rosei, *Science* **2005**, *309*, 752; b) S. Torbrügge, M. Reichling, A. Ishiyama, S. Morita, O. Custance, *Phys. Rev. Lett.* **2007**, *99*, 0561001; c) M. V. Ganduglia-Pirovano, J. L. F. Da Silva, J. Sauer, *Phys. Rev. Lett.* **2009**, *102*, 026101.

[5] a) H.-X. Mai, L.-D. Sun, Y.-W. Zhang, R. Si, W. Feng, H.-P. Zhang, H.-C. Liu, C.-H. Yan, *J. Phys. Chem. B* **2005**, *109*, 24380; b) P. Martin, S. C. Parker, D. C. Sayle, G. W. Watson, *Nano Lett.* **2007**, *7*, 543; c) S. Dai, W. Zili, Z.-A. Quiao, *ChemSusChem* **2013**, *6*, 1821.

[6] a) M. Nolan, S. C. Parker, G. W. Watson, *Surf. Sci.* **2005**, *595*, 223; b) T. X. T. Sayle, M. Cantoni, U. M. Bhatta, S. C. Parker, S. R. Hall, G. Mobus, M. Molinari, D. Reid, S. Seal, D. C. Sayle, *Chem. Mater.* **2012**, *24*, 1811.

[7] a) G. Vilé, B. Bridier, J. Wichert, J. Pérez-Ramírez, *Angew. Chem.* **2012**, *124*, 8748; *Angew. Chem. Int. Ed.* **2012**, *51*, 8620; b) G. Vilé, S. Wrabetz, L. Floryan, M. E. Schuster, F. Girgsdies, D. Teschner, J. Pérez-Ramírez, *ChemCatChem* **2014**, *6*, 1928.

[8] a) J. Carrasco, G. Vilé, D. Fernández-Torre, R. Pérez, J. Pérez-Ramírez, M. V. Ganduglia-Pirovano, *J. Phys. Chem. C* **2014**, *118*, 5352; b) M. García-Melchor, N. López, *J. Phys. Chem. C* **2014**, *118*, 10921.

[9] Z. L. Wang, X. D. Feng, *J. Phys. Chem. B* **2003**, *107*, 13563.

[10] a) E. Aneggi, J. Llorca, M. Boaro, A. Trovarelli, *J. Catal.* **2005**, *234*, 88; b) M. Huang, S. Fabris, *J. Phys. Chem. C* **2008**, *112*, 8643.